Check for updates

Chemistry–A European Journal

Research Article
doi.org/10.1002/chem.202200948

Chemistry Europe
European Chemical Societies Publishing

www.chemeurj.org

Pressure Effects on 3d^n (n = 4, 9) Insulating Compounds: Long Axis Switch in Na_3MnF_6 not Due to the Jahn-Teller Effect

Inés Sánchez-Movellán,*[a] David Carrasco-Busturia,[b] Juan M. García-Lastra,[b] Pablo García-Fernández,[a] José A. Aramburu,[a] and Miguel Moreno[a]

Abstract: The pressure-induced switch of the long axis of MnF_6^{3-} units in the monoclinic Na_3MnF_6 compound and Mn^{3+}-doped Na_3FeF_6 is explored with the help of first principles calculations. Although the switch phenomenon is usually related to the Jahn-Teller effect, we show that, due to symmetry reasons, it cannot take place in 3d^n (n = 4, 9) systems displaying a static Jahn-Teller effect. By contrast, we prove that in Na_3MnF_6 the switch arises from the anisotropic response of the low symmetry lattice to hydrostatic pressure. Indeed, while the long axis of a MnF_6^{3-} unit at ambient pressure corresponds to the Mn^{3+}–F_3^- direction, close to the crystal *c* axis, at 2.79 GPa the *c* axis is reduced by 0.29 Å while *b* is unmodified. This fact is shown to force a change of the HOMO wavefunction favoring that the long axis becomes the Mn^{3+}–F_2^- direction, not far from crystal *b* axis, after the subsequent relaxation process. The origin of the different *d-d* transitions observed for Na_3MnF_6 and CrF_2 at ambient pressure is also discussed together with changes induced by pressure in Na_3MnF_6. The present work opens a window for understanding the pressure effects upon low symmetry insulating compounds containing d^4 or d^9 ions.

Introduction

In insulating compounds containing d^4 or d^9 transition metal cations in sixfold coordination, remarkable changes in the geometry of associated complexes are induced by external pressure. This singular behavior has been observed, for instance, in Na_3MnF_6,[1] $(NH_4)_2Cu(H_2O)_6(SO_4)_2$,[2] $Cs_2Zn(ZrF_6)_2\cdot 6H_2O:Cu^{2+}$,[3] $CuF_2(H_2O)_2(pyz)$[4] (pyz = pyrazine) or $CuWO_4$,[5] and it has systematically been related[1–8] to both the existence of a static Jahn-Teller (JT) effect and a pressure-induced switch of the principal axis of the complex formed by the 3d^n (n = 4, 9) cation.

Nonetheless, this explanation, though widely followed, is hard to accept first due to the restrictive symmetry conditions necessary for the presence of a JT effect.[9,10] Indeed, the JT effect requires the existence of an *initial* geometry where the ground state of the complex is actually degenerate. This condition is fulfilled under cubic or trigonal symmetry,[9] and thus a static JT effect has been observed in cases like $KZnF_3$:Cu^{2+},[11–13] d^9 ions (Ni^+, Cu^{2+}, Ag^{2+}) doped NaCl,[14–20] $A(H_2O)_6SiF_6:Cu^{2+}$ (A = Mg, Zn)[21–23,17] or AgF_2[24,25] but not in K_2ZnF_4:Cu^{2+}[26] where the host lattice is tetragonal.[27] This key argument thus makes difficult to assume the existence of a JT effect in crystals like Na_3MnF_6, $(NH_4)_2Cu(H_2O)_6(SO_4)_2$, $CuF_2(H_2O)_2(pyz)$, or $CuWO_4$, whose structures are either monoclinic or triclinic.[1–8]

Furthermore, in systems displaying a static JT effect, a hydrostatic pressure can hardly switch the principal axis direction. Indeed, for a Cu^{2+} ion in a cubic crystal like the $KZnF_3$ perovskite,[11–13] the principal axis of the CuF_6^{4-} unit can be one of the three C_4 axes (along X, Y, Z directions) of the lattice as a result of a static JT effect that leads to a local *tetragonal* symmetry. This symmetry breaking ultimately arises from the unavoidable *random strains* present in any real crystal, a key point firstly clarified by Ham.[9,10] Accordingly, if in a given region of the $KZnF_3$ cubic crystal the principal axis of the CuF_6^{4-} complex is forced to be Z by random strains, the X and Y axes continue to be equivalent under hydrostatic pressure, which is an isotropic stress. Thus, an applied pressure can modify the value of the tetragonal distortion and the JT stabilization energy, E_{JT}, but not the principal direction of the CuF_6^{4-} unit at a given point of the crystal. In contrast, systems that do not present a JT effect display preferential directions that, as we will show, are associated with the elastic properties of the lattice. Armed with this knowledge, gained for example using closed-shell systems that are clearly not suspect of displaying the JT

---

[a] I. Sánchez-Movellán, Dr. P. García-Fernández, Prof. J. A. Aramburu,
Prof. M. Moreno
Departamento de Ciencias de la Tierra y Física de la Materia Condensada
Universidad de Cantabria
Avenida de los Castros s/n, 39005
Santander (Spain)
E-mail: sanchezi@unican.es

[b] Dr. D. Carrasco-Busturia, Prof. J. M. García-Lastra
Department of Energy Conversion and Storage
Technical University of Denmark
Anker Engelunds Vej. Building 301,
2800 Kgs. Lyngby (Denmark)

© 2022 The Authors. Chemistry - A European Journal published by Wiley-VCH GmbH. This is an open access article under the terms of the Creative Commons Attribution Non-Commercial License, which permits use, distribution and reproduction in any medium, provided the original work is properly cited and is not used for commercial purposes.

© 2022 The Authors. Chemistry - A European Journal published by Wiley-VCH GmbH

effect, one may predict the possible change in direction of the long axis of these transition-metal complexes. This makes JT and non-JT systems quite different since in the first class there cannot be a systematic long-axis switch while in the second class this can be allowed.

Bearing these facts in mind, it has previously been shown that in low symmetry compounds like CuF_2, CrF_2, or K_2CuF_4 there is no JT effect.[28,29] Therefore, the local distortion and the ground state of involved MF_6^{4-} (M = Cu, Cr) units obey to different causes that can be uncovered with the help of first principles calculations. Such an analysis stresses the importance of considering the effects of the anisotropy of the low symmetry lattice on the complex. In fact, even if the MF_6^{4-} (M = Cu, Cr) complex is, in principle, octahedral the anisotropic electric field due to the rest of lattice ions generally leads to a non-degenerate ground state.[13,17,26,29] Moreover, that anisotropy makes that the six F^- ligands are no longer elastically equivalent, and thus the change of the force constant due to the rest of the lattice can be different for each of the involved ligands. Both facts have been proved to play a key role in explaining the different distortion and ground state observed[30,31] for Cu^{2+} or Ni^+ in the layered lattices K_2MgF_4 and K_2ZnF_4.[32,26]

According to the present arguments, it is now necessary to understand why in low symmetry compounds involving $3d^n$ (n = 4, 9) cations the nature of the longest local axis of the involved complex can be switched by an applied pressure if that phenomenon is not due to a JT effect. Seeking to gain a better insight on this relevant issue, this work focuses on the monoclinic Na_3MnF_6 compound[1,6,7] where pressure effects have been investigated experimentally.[1] This compound is taken as a guide for the present study, carried out with the help of first principles calculations and an analysis of available experimental results.

The singularity of $3d^n$ (n = 4, 9) compounds displaying a sixfold coordination just reflects that the ground state electronic density of a MX_6 unit (M = $3d^4$ or $3d^9$ ion), has not a cubic symmetry and thus, if all ligands are at the same distance, not all of them experience the same force.[26,33] However, this *general* behavior does not appear in high spin MX_6 complexes when M is a cation like Fe^{3+}, Mn^{2+} (d^5) or Cr^{3+} (d^3) whose ground state electronic density is close to spherical. For this reason, in the study of Na_3MnF_6 it is also useful to explore how the structure evolves when all Mn^{3+} cations are replaced by a cation with a similar ionic radius but a more spherical electronic density, keeping the same space group. This is just the so-called *parent phase* previously used[24,28,29] as a good starting point for understanding the structure and ground state of compounds like AgF_2, CuF_2, CrF_2, or K_2CuF_4.

This work is organized as follows. In section 2 we describe the crystal structure of Na_3MnF_6 as a function of pressure observed experimentally. For the sake of clarity, it is compared to that of cryolite (Na_3AlF_6) at ambient pressure.[34] The computational tools used in the present study are explained in section 3, while main results are given in section 4. Some final remarks are provided in the last section.

Crystal structure of Na_3MnF_6 under pressure: Experimental results

According to Englich et al. the structure of Na_3MnF_6 at ambient pressure can be described[6] by the monoclinic space group $P2_1/n$, a non-standard setting more visual than the standard one, $P2_1/c$. A view of the corresponding lattice cell is displayed in Figure 1, whereas the ensemble of lattice parameters (a, b, c, and monoclinic angle, β) and Mn^{3+}–F^- distances is reported in Table 1. When pressure increases up to 2.79 GPa, the space group of Na_3MnF_6 is unmodified,[1] being again $P2_1/n$. The structure observed experimentally at P = 2.79 GPa is also shown in Figure 1. The crystal data derived[1] by Carlson et al. at P = 0.12 GPa and P = 2.79 GPa are collected in Table 1, together with those corresponding to the cryolite compound (Na_3AlF_6) at zero pressure,[34] also displaying a $P2_1/n$ space group.

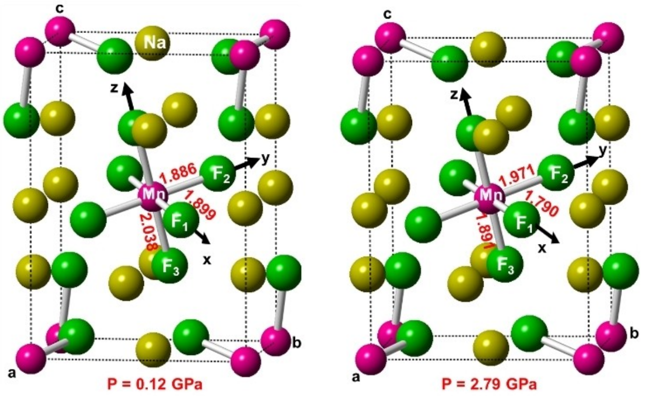

Figure 1. Experimental unit cells of Na_3MnF_6 compound at pressures P = 0.12 and 2.79 GPa in the non-standard monoclinic $P2_1/n$ setting.[1] {x,y,z} are the local axes of the MnF_6^{4-} complexes, with C_i point symmetry. The 3 Mn–F_i distances (in Angstroms) are also shown.

Table 1. Description of the crystal structure of Na_3MnF_6 reported at P = 0 GPa by Englich et al.[6] and at P = 0.12 and 2.79 GPa by Carlson et al.[1] In addition to lattice parameters (a, b, c and monoclinic angle, β), the values of three Mn^{3+}–F^- distances, R_1, R_2 and R_3, are also given. In a first approximation, it can be considered that the directions of R_1, R_2 and R_3 are parallel to *a*, *b* and *c* axis, respectively. The value of the longest metal-ligand distance is written in bold type for each structure. For comparison, the values corresponding to Na_3AlF_6[34] are also shown. All distances are in Å and the β angle in degrees.

Compound	Pressure	a	b	c	β	R_1	R_2	R_3
Na_3MnF_6	0	5.471	5.683	8.073	88.96	1.862	1.897	**2.018**
	0.12	5.470	5.690	8.066	89.08	1.899	1.886	**2.038**
	2.79	5.386	5.690	7.783	90.76	1.790	**1.971**	1.891
Na_3AlF_6	0	5.402	5.596	7.756	90.27	1.804	**1.813**	1.805

© 2022 The Authors. Chemistry - A European Journal published by Wiley-VCH GmbH

15213765, 2022, 43, Downloaded from https://chemistry-europe.onlinelibrary.wiley.com/doi/10.1002/chem.202200948 by Universidad De Cantabria, Wiley Online Library on [21/03/2024]. See the Terms and Conditions (https://onlinelibrary.wiley.com/terms-and-conditions) on Wiley Online Library for rules of use; OA articles are governed by the applicable Creative Commons License

As shown in Table 1, the crystallographic data obtained at ambient pressure and at 0.12 GPa are practically identical. They reveal that the lattice cell is nearly orthorhombic with a monoclinic angle $\beta = 89°$. The MnF_6^{3-} complexes formed in Na_3MnF_6 are practically isolated, i.e., they do not share F^- ligands and the distance between two neighbors Mn^{3+} cations is equal to 5.40 Å. As the F^-–Mn^{3+}–F^- angle for two F^- ions in cis position[1,6] differs by about 2° from 90°, the local symmetry of a MnF_6^{3-} complex is triclinic C_i. The three Mn^{3+}–F_i^- lines (i = 1, 2, 3) in Figure 1 are not strictly parallel to the crystallographic *a, b*, and *c* axes, respectively, due to a tilting of the complex. Still, the Mn–F_3 line is mainly oriented along the *c* axis and the Mn–F_2 line along the *b* axis. For instance, the angle between *c* axis and the Mn–F_3 direction is equal to 22°. The three Mn^{3+}–F^- distances are not equal; the largest one, R_3, corresponds to the Mn–F_3 bond and differs from R_2 by 0.152 Å, while R_2 and R_1 are identical within 1.5 % (Table 1).

The results for Na_3MnF_6 at zero pressure are somewhat similar to those for Na_3AlF_6,[34] also displayed in Table 1. Indeed, despite Al^{3+} being a closed shell cation, the three Al^{3+}–F^- distances are not equal, although the differences among them are smaller than 0.01 Å. On the other hand, in the cryolite the largest Al^{3+}–F^- distance corresponds to R_2 and not to R_3, at variance with Na_3MnF_6 at ambient pressure (Table 1). Interestingly, when we compare the lattice parameters of Na_3MnF_6 at ambient pressure with those for Na_3AlF_6 the reduction is not isotropic. Indeed, *c* reduces by 4 % while *b* and *a* decrease by less than 1.5 %.

An increase of pressure reduces the value of lattice parameters, specially *c*. So, on passing from P = 0 to P = 0.91 GPa the value of *c* decreases by 0.081 Å according to experimental data[1] by Carlson et al. At the same time, the value of R_3-R_2 at P = 0.91 GPa is equal only to 0.081 Å[1] in comparison to R_3-R_2 = 0.121 Å at ambient pressure (Table 1). As a salient feature, Na_3MnF_6 undergoes a phase transition[1] at about 2.2 GPa, where the lattice parameter *c* abruptly decreases by about 2 %. Moreover, it is a first-order phase transition because is isosymmetric (the space group is always $P2_1/n$) and involves a significant hysteresis[1] of ~0.8 GPa. Despite this fact, the phase transition is characterized by a switch of the longest axis of all MnF_6^{3-} complexes. Indeed, while at ambient pressure that axis corresponds to the Mn^{3+}–F_3^- direction, it is the Mn^{3+}–F_2^- direction that becomes the longest axis after the phase transition, such as it is shown in Table 1. Furthermore, comparing the experimental results at different pressures, we can notice that, on passing from P = 0 GPa to P = 2.79 GPa the three lattice parameters evolve in a very different way: *c* is reduced by 0.29 Å while *b* is unmodified and *a* decreases only by 0.08 Å (Table 1).

The origin of the switch of the longest axis under pressure is discussed in Section 4 helped by the results of first principles calculations. In that analysis, particular attention is paid to exploring the electronic density changes due to pressure.

Computational tools

First principles periodic calculations have been performed on pure Na_3MnF_6, its parent phase Na_3FeF_6, as well as on doped $Na_3FeF_6{:}Mn^{3+}$ by means of the CRYSTAL17 code. This software works with linear combinations of Gaussian type functions to represent the Bloch orbitals.[35]

All electron triple-zeta polarized basis set of high quality developed by Peitinger et al.[36,37] were employed, together with the one-parameter hybrid functionals B1WC and PW1PW, which include 16 % and 20 % of Hartree-Fock exchange, respectively, and have provided accurate results for crystalline structures and properties of insulating systems containing transition metal ions.[37,38]

First, we have optimized the geometry of the two phases that exist in Na_3MnF_6, at ambient pressure, and at P = 2.79 GPa, at the monoclinic $P2_1/n$ space group, obtaining that both lattice parameters and bond Mn–F distances are similar to the experimental data, with discrepancies of less than 3.5 %. The sampling of reciprocal space for the numerical integration within the Brillouin zone was 8x8x8 Monkhorst-Pack grid, which represents a distance between two consecutive k points of 0.144, 0.138 and 0.072 $Å^{-1}$ conforming to the three reciprocal space directions. For geometry optimizations the tolerance for energy change was 10^{-8} Hartree and for gradient and nuclei displacement were 0.0002 a.u.

The next step was the optimization of the parent phase structure. Regarding this calculation, all open shell Mn^{3+} ions, with d^4 electronic configuration and S = 2, were replaced by Fe^{3+} ions (d^5 electronic configuration and S = 5/2) with spherical density (in vacuo) and equal ionic radius, $r(Mn^{3+}) \approx r(Fe^{3+}) \approx 0.785$ Å.[39] The symmetry of the optimized parent phase Na_3FeF_6 remains in the same $P2_1/n$ space group but the complexes are less distorted, reflecting a more spherical symmetry for Fe^{3+} in Na_3FeF_6 than for Mn^{3+} in Na_3MnF_6. Further discussion on this issue is provided in Section 4.2.

In addition, cluster simulations on MnF_6^{3-} complexes have been performed in order to explore the relationship between the structural changes due to pressure and the variations undergone by the HOMO as well as the influence of pressure on the spin allowed *d-d* transitions. These calculations have been carried out by means of the Amsterdam density functional (ADF) code,[40] which works with DFT techniques in the Kohn-Sham framework. Hybrid B3LYP functional (25 % of exact exchange) combined with triple zeta polarized basis set have been employed in the simulations. The core electrons (1s-3p for Mn^{3+}, 1 s for F^-) were kept frozen since they do not play a relevant role in the effects we focus on. In these calculations, the MnF_6^{3-} clusters were embedded in the electrostatic potential of the rest of lattice ions,[41,42] which was previously calculated through Ewald-Evjen summations.[43,44] Although the effects of this internal potential are important in systems like ruby,[45–47] the Egyptian-blue pigment[48] or $K_2ZnF_4{:}Cu^{2+}$,[13,26,32] it is not the case of Na_3MnF_6 where only induces energy variations in the optical *d-d* transitions equal or smaller than 0.1 eV. Such transitions are discussed in Section 4.4. Both complex and environment were rotated in such a way that the directions R_1,

© 2022 The Authors. Chemistry - A European Journal published by Wiley-VCH GmbH

15213765, 2022, 43, Downloaded from https://chemistry-europe.onlinelibrary.wiley.com/doi/10.1002/chem.202200948 by Universidad De Cantabria, Wiley Online Library on [21/03/2024]. See the Terms and Conditions (https://onlinelibrary.wiley.com/terms-and-conditions) on Wiley Online Library for rules of use; OA articles are governed by the applicable Creative Commons License

15213765, 2022, 43, Downloaded from https://chemistry-europe.onlinelibrary.wiley.com/doi/10.1002/chem.202200948 by Universidad De Cantabria, Wiley Online Library on [21/03/2024]. See the Terms and Conditions (https://onlinelibrary.wiley.com/terms-and-conditions) on Wiley Online Library for rules of use; OA articles are governed by the applicable Creative Commons License

Table 2. Calculated values of lattice parameters (a, b, c and β) and the three Mn^{3+}–F^- distances, R_1, R_2, R_3, for Na_3MnF_6 in the $P2_1/n$ space group at both zero pressure and P = 2.79 GPa. The results are compared to available experimental results.[1,6] The value of the longest Mn^{3+}–F^- distance is written in bold type for both pressures. All distances are in Å and the β angle in degrees.

P		a	b	c	β	R_1	R_2	R_3
0	Experimental	5.471	5.683	8.073	88.96	1.862	1.897	**2.018**
	Calculated	5.460	5.646	8.137	88.47	1.864	1.880	**2.069**
2.79	Experimental	5.386	5.690	7.783	89.24	1.790	**1.971**	1.891
	Calculated	5.381	5.720	7.713	88.37	1.861	**2.041**	1.866

R_2 and R_3 lies, approximately, along the local axes *x*, *y* and *z* respectively.

Understanding the long axis switch induced by pressure in Na_3MnF_6 entails the analysis of the wavefunction in the ground state at different stages since its evolution leads to the distortions observed in this system. Therefore, the HOMO wavefunction has been determined for Na_3MnF_6 at different pressures and also for Na_3FeF_6:Mn^{3+}. In the latter case, the HOMO corresponding to the MnF_6^{3-} unit has been derived for both the undistorted parent phase and the final equilibrium geometry. In these calculations, the wavefunction coefficients have been obtained following Mulliken population criterion.

Results and Discussion: Na_3MnF_6

Results of calculations at P = 0 and P = 2.79 GPa for Na_3MnF_6

The optimized geometries for Na_3MnF_6 obtained under periodic boundary conditions working in the $P2_1/n$ space group are collected in Table 2 for P = 0 and 2.79 GPa. Such results are compared to available experimental results.[1,6] The calculated values reasonably reproduce the experimental results. Indeed, calculated lattice parameters deviate from experimental ones less than 1 % while the error on the value of the longest Mn^{3+}–F^- distance is smaller than 3.5 %. It is worth noting that the present calculations also lead to the long axis along the Mn^{3+}–F_3^- direction at zero pressure while it is along the Mn^{3+}–F_2^- direction for P = 2.79 GPa. Moreover, they also shed light on the nature of the ground state of the MnF_6^{3-} complex at both pressures.

The electronic ground state of a *hypothetically* octahedral (O_h point group) MnF_6^{3-} unit with S = 2 corresponds to the configuration $t_{2g}^3e_g^1$. At zero pressure, the present periodic and cluster calculations on Na_3MnF_6 reveal that the unpaired electron coming from e_g has a dominant $3z^2$-r^2 character where z essentially reflects the Mn^{3+}–F_3^- direction (Figure 1). This is consistent with R_3 being the long axis while R_1 and R_2 are equal within 1.5 %. Indeed, if the octahedron is elongated along the z axis and $R_1 = R_2$ the HOMO corresponds to a *molecular orbital* $|3z^2\text{-}r^2\rangle$ (transforming like $3z^2$-r^2) while the LUMO corresponds to $|x^2\text{-}y^2\rangle$. This situation is thus quite similar to that found for the low spin (S = 1/2) $RhCl_6^{4-}$ complex generated by the d^7 Rh^{2+} cation formed in NaCl.[49,50]

At P = 2.79 GPa the present calculations reveal that the unpaired electron coming from e_g has a dominant $3y^2$-r^2 character where y essentially reflects the Mn^{3+}–F_2^- direction (Figure 1). Thus, the switch of the longest axis also involves a change of the nature of the HOMO orbital helped by the anisotropic reduction of lattice parameters under pressure (Table 2). As the biggest reduction occurs for the *c* axis while the *b* axis is practically unmodified one can already envisage that the electronic density in the HOMO prefers to be oriented along the Mn^{3+}–F_2^- direction and then push F_2 ligands away.

The change of the calculated electronic spin density (difference between spin up and spin down densities) when pressure moves from P = 0 GPa to 2.79 GPa is depicted in Figure 2. These spin density contours corresponds to a good extent to the four electrons placed in the $|3z^2\text{-}r^2\rangle$, $|xy\rangle$, $|xz\rangle$, $|yz\rangle$ orbitals all of them with spin up. At P = 0 GPa, Figure 2 shows the existence of bonding with $2p_\sigma$ and 2 s orbitals of F_3^- ligands placed on the z axis of the MnF_6^{3-} complexes, consistent with an unpaired electron from e_g with a dominant $3z^2$-r^2 character. By contrast, at P = 2.79 GPa that bonding involves F_2^- ligands placed on the y local axis of the complexes. A further discussion on this issue is given in Section 4.3.

Results on the parent phase Na_3FeF_6 pure and doped with Mn^{3+} at zero pressure

In the study of a d^n (n = 4, 9) compounds it has proved to be useful to determine the actual structure once each cation is replaced by another one with a similar ionic radius but a more spherical electronic density.[24,28,29,33,51] As during this process, giving rise to the so-called parent phase, the space group does not change, the symmetry of the parent phase is necessarily equal or higher than that of the initial d^n (n = 4, 9) compound. For example, for CuF_2 (monoclinic $P2_1/n$ space group) the $Cu^{2+} \rightarrow Zn^{2+}$ substitution leads to a ZnF_2 parent phase belonging to the tetragonal $P4_2/mnm$ space group.[51] Accordingly, the rutile structure of ZnF_2 becomes unstable[51] as far as Zn^{2+} ions are progressively substituted by Cu^{2+}.

In the present case of Na_3MnF_6, the parent phase is obtained by substituting all Mn^{3+} ions by Fe^{3+} ones (both with the same ionic radius, 0.785 Å[39]). A geometry optimization calculation performed on the Na_3FeF_6 parent phase, starting from the experimental $P2_1/n$ geometry of Na_3MnF_6, led to a structure displaying the *same* $P2_1/n$ space group (Table 3). Moreover, that phase actually corresponds to the experimental Na_3FeF_6 compound, whose structure at ambient pressure was firstly reported by Croft and Kestigian from X-ray diffraction in powder.[52] The values of lattice parameters obtained by these authors are gathered on Table 3 and compared to results of

© 2022 The Authors. Chemistry - A European Journal published by Wiley-VCH GmbH

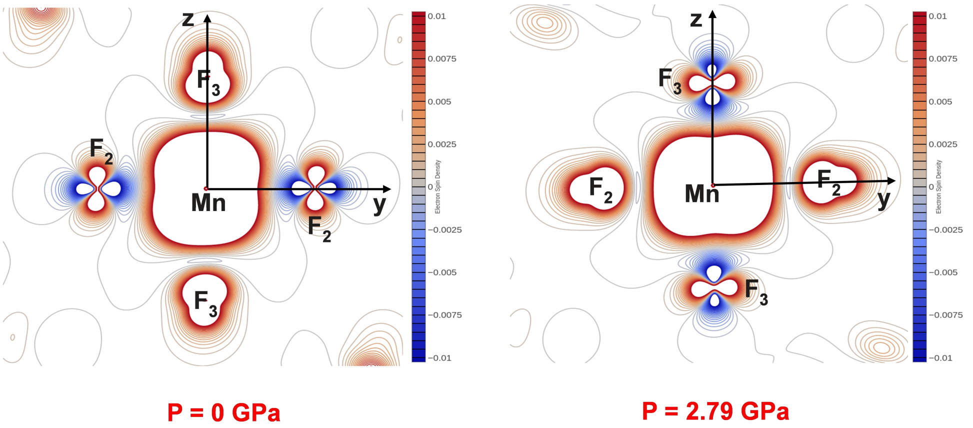

Figure 2. Calculated electronic spin density (difference between spin up and spin down densities) of the ground state of a MnF_6^{3-} unit in Na_3MnF_6 when pressure moves from P = 0 GPa to 2.79 GPa. At P = 0 GPa results reflect an antibonding orbital involving the $3z^2$-r^2(Mn) orbital mixed with with $2p_\sigma$(F) and 2 s(F) orbitals of F_3^- ligands. By contrast, at P = 2.79 GPa that orbital involves orbitals of F_2^- ligands. Note that as calculations are spin unrestricted there are small regions with negative spin density (blue colour) showing the polarization of fully occupied bonding orbitals by the four unpaired electrons with spin up.

Table 3. Experimental values of lattice parameters (a, b, c and β) derived from X-ray diffraction power data for Na_3FeF_6 at ambient pressure displaying the $P2_1/n$ space group.[52] Such values are compared to the structural information obtained from present geometry optimizations for the parent phase of Na_3MnF_6 where the three Fe^{3+}–F^- distances have been determined. All distances are in Å and the β angle in degrees.

	a	b	c	β	R_1	R_2	R_3
Experimental	5.506	5.719	7.925	90.5	–	–	–
Calculated	5.483	5.720	7.936	89.5	1.931	1.945	1.943

Table 4. Calculated values of three metal-ligand distances, R_1, R_2 and R_3, obtained for a Mn^{3+} impurity in the Na_3FeF_6 parent phase using two different sets of lattice parameters, those optimized for Na_3FeF_6 (second row) and other set where the value of *c* increases only by 1.1 % (third row). It can be noticed that in the latter case, the longest axis is along the Mn^{3+}–F_3^- direction and not along the Mn^{3+}–F_2^- direction. The results for pure Na_3FeF_6 (first row) are also included for comparison. In every case the longest metal-ligand distance is written in bold. All distances are in Å and the β angle in degrees.

	a	b	c	β	R_1	R_2	R_3
Na_3FeF_6	5.483	5.720	7.936	89.5	1.931	**1.945**	1.943
Na_3FeF_6:Mn^{3+}	5.483	5.720	7.936	89.5	1.856	**2.045**	1.895
Na_3FeF_6:Mn^{3+}	5.490	5.700	8.020	89.5	1.866	1.892	**2.049**

present geometry optimization. Both sets of data are essentially coincident. However, Croft and Kestigian in their powder study did not report the values of metal-ligand distances[52] and thus we cannot compare them to those derived from present calculations (Table 3).

The local symmetry around a Fe^{3+} cation in Na_3FeF_6 is given by the same triclinic C_i point group as that for Mn^{3+} in Na_3MnF_6. Despite this fact, it should be noticed that R_2-R_3 = 0.002 Å derived for Na_3FeF_6 is clearly smaller than R_2-R_3 = 0.180 Å determined for Na_3MnF_6 at 2.79 GPa (Table 2). This situation is thus rather similar to that found for cryolite (Table 1) where the longest Al^{3+}–F^- distance also corresponds to R_2 and R_2-R_3 = 0.008 Å.

Particular attention has been paid to study the behavior of a single substitutional Mn^{3+} impurity in Na_3FeF_6. Results of the present calculations are gathered in Table 4. Although the Fe^{3+} → Mn^{3+} substitution does not modify the C_i local symmetry, it enhances the octahedron distortion leading to a local geometry that resembles that derived for pure Na_3MnF_6 at 2.79 GPa (Table 2) with R_2-R_3 = 0.15 Å. Therefore, the Fe^{3+} → Mn^{3+} substitution does not give rise to any symmetry breaking, such as it happens in a static JT effect. Nevertheless, the increase of R_2-R_3 on passing from pure Na_3FeF_6 (R_2-R_3 = 0.002 Å) to Na_3FeF_6:Mn^{3+} (R_2-R_3 = 0.15 Å) has to be related to the different ground state electronic density in the corresponding FeF_6^{3-} and MnF_6^{3-} units.

Let us consider an *initial step* where Mn^{3+} replaces Fe^{3+} in the *undistorted* Na_3FeF_6 lattice. We have verified that in that situation the unpaired electron coming from e_g has a dominant $3y^2$-r^2 character such as it is shown in Table 5. Indeed, the calculated wavefunction of the HOMO, $|\psi_H\rangle$, can shortly be written as

$$|\psi_H\rangle = 0.972|3y^2\text{-}r^2\rangle + 0.234|x^2\text{-}z^2\rangle \qquad (1)$$

Table 5. Relevant data corresponding to a Mn^{3+} impurity in Na_3FeF_6. In the initial step, a Mn^{3+} ion just substitutes a Fe^{3+} one in the *undistorted* Na_3FeF_6 parent lattice, while the final step describes the equilibrium geometry of a single Mn^{3+} impurity in the parent phase. In both situations, the calculated wavefunction of the HOMO and the value of the HOMO-LUMO gap, Δ, are given. The *relative* energy of the electronic ground state (GS) derived for both situations is also reported. All distances are in Å and energies in eV.

Step	R_1, R_2, R_3	HOMO	Δ	GS energy
Initial	1.931, 1.945, 1.943	$0.972\,|3y^2\text{-}r^2> + 0.234\,|x^2\text{-}z^2>$	0.06	0
Final	1.856, 2.045, 1.895	$0.996\,|3y^2\text{-}r^2> + 0.078\,|x^2\text{-}z^2>$	0.76	−0.18

© 2022 The Authors. Chemistry - A European Journal published by Wiley-VCH GmbH

15213765, 2022, 43, Downloaded from https://chemistry-europe.onlinelibrary.wiley.com/doi/10.1002/chem.202200948 by Universidad De Cantabria, Wiley Online Library on [21/03/2024]. See the Terms and Conditions (https://onlinelibrary.wiley.com/terms-and-conditions) on Wiley Online Library for rules of use; OA articles are governed by the applicable Creative Commons License

Here $|3y^2\text{-}r^2\rangle$ just means a *molecular orbital* of the MnF_6^{3-} unit transforming like $3y^2\text{-}r^2$. Accordingly, the LUMO is mainly made of $|x^2\text{-}z^2\rangle$, and it is placed only at 0.06 eV above the HOMO just reflecting that in this initial step the local symmetry of the MnF_6^{3-} unit is C_i despite the three Mn^{3+}–F^- distances are equal within 0.01 Å. These facts thus stress that in this initial stage the electronic ground state of the MnF_6^{3-} unit is not degenerate, thus excluding the existence of a JT effect.[13] Despite this fact, as the electron placed in the HOMO is described by Equation (1), it exerts a different force on the three kinds of ligands initially placed at the same distance from Mn^{3+} within 0.01 Å. A different situation holds, however, when we consider the *average* $(3y^2\text{-}r^2)^{0.5}(x^2\text{-}z^2)^{0.5}$ configuration, whose associated electronic density leads to a similar force on all ligands.[26,33,53] Accordingly, in the actual $(3y^2\text{-}r^2)^1(x^2\text{-}z^2)^0$ configuration, the *difference* of electronic density pushes the F_2 ligands away while it tends to approach F_1 and F_3 ligands, such as it is shown in Tables 4 and 5. This relaxation process, leading to the final equilibrium geometry of a single MnF_6^{3-} unit in the parent phase, involves an energy gain, E_R, calculated to be equal to 0.18 eV (Table 5).

In addition to study the behavior of a Mn^{3+} impurity in Na_3FeF_6, we have also investigated the influence of a small increase (1.1 %) on the *c* lattice parameter upon both the equilibrium geometry and the electronic ground state of the MnF_6^{3-} unit. The results, also displayed in Table 4, show that under that 1.1 % increase on the *c* parameter the longest distance of the MnF_6^{3-} unit changes from being R_2 to R_3 and in the final geometry the unpaired electron coming from e_g has then a dominant $3z^2\text{-}r^2$ character.

Understanding the long axis switch induced by pressure in Na_3MnF_6

Bearing the analysis carried out in sections 4.1 and 4.2 in mind, the long axis switch in Na_3MnF_6 appears to arise from the significant anisotropic response of this compound to hydrostatic pressure. Thus, although the pressure on any crystal face is always the same, the reduction of crystal parameters is far from being isotropic. Indeed, in the pressure range 0–2 GPa the lattice parameters *a* and, specially, *c*, experience a progressive decrease, while *b* is nearly unmodified.[1] This pressure reduction of *c* and *a* tends, in turn, to reduce the value of R_3 and R_1, as it is experimentally shown. For instance, at $P = 0.91$ GPa, $R_3 = 1.978$ Å and $R_1 = 1.810$ Å,[1] which are clearly smaller than those reported at 0.12 GPa (Table 1). By contrast, the value $R_2 = 1.897$ Å measured at $P = 0.91$ GPa[1] is only 0.01 Å *higher* than the value obtained at 0.12 GPa (Table 1).

A progressive reduction of R_3 approaches the two F_3^- ligands to Mn^{3+}, thus increasing the energy of the $|3z^2\text{-}r^2\rangle$ level, which works against having the HOMO of the MnF_6^{3-} unit in Na_3MnF_6 with a dominant $3z^2\text{-}r^2$ character. For this reason, when pressure increases, it appears more favorable a change of the HOMO wavefunction in order to reach a dominant $3y^2\text{-}r^2$ character and placing the associated density along the *y* direction where R_2 is not reduced by pressure. Moreover, although this switch of the HOMO wavefunction involves, in principle, an energy increase there is an energy reduction in the subsequent relaxation process leading to an increase of R_2 and a decrease of R_3 (Table 2).

The main steps of this process induced by pressure in Na_3MnF_6 can quantitatively be clarified looking at Figure 3. Particular attention is paid to analyze, in each step, the shape of the HOMO wavefunction of the MnF_6^{3-} unit, $|\psi_H\rangle$. In general, according to calculations, $|\psi_H\rangle$ can simply be written as follows

$$|\psi_H\rangle = \alpha|3z^2\text{-}r^2\rangle + \beta|x^2\text{-}y^2\rangle \tag{2}$$

with $\alpha^2 + \beta^2 = 1$. Four steps are considered in Figure 3. The initial step I describes the situation of a MnF_6^{3-} unit in Na_3MnF_6 at ambient pressure, while step II reflects the experimental geometry[1] and HOMO wavefunction at about $P = 1.8$ GPa where the longest axis is still R_3, as described by our first principles simulations. Similarly, step IV corresponds with data at $P = 2.79$ GPa pressure, where the longest axis is already R_2. Step III is a *virtual process* where the geometry is that of step II ($P = 1.8$ GPa) while the HOMO wavefunction has been switched to that of the final step ($P = 2.79$ GPa). We describe below the process to obtain its energy.

At ambient pressure, the MnF_6^{3-} unit is elongated along the z axis while R_1 and R_2 are identical within 0.03 Å. Accordingly, the HOMO wavefunction is essentially $|3z^2\text{-}r^2\rangle$ ($\beta \approx 0$). On passing from step I to step II, R_3 decreases while R_2-R_1 increases. This favors an increase of the $|x^2\text{-}y^2\rangle$ component although $|\psi_H(\mathrm{II})\rangle$ still exhibits a dominant $|3z^2\text{-}r^2\rangle$ contribution (84.2 %) and is described by

$$|\psi_H(\mathrm{II})\rangle = 0.917|3z^2\text{-}r^2\rangle + 0.397|x^2\text{-}y^2\rangle \tag{3}$$

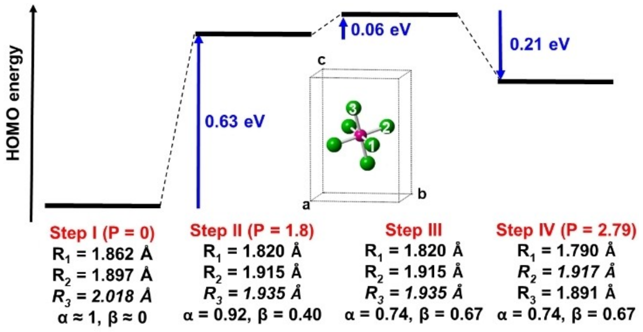

Figure 3. Relative variation of both energy and wavefunction of the HOMO for MnF_6^{3-} complexes in Na_3MnF_6 calculated at different values of metal-ligand distances, whose directions in the Na_3MnF_6 unit cell are also shown. Step I corresponds to R_i (i = 1, 2, 3) values for zero pressure while step II reflects the experimental geometry at about 1.8 GPa and step IV that for a pressure of 2.79 GPa where the highest metal-ligand distance is already R_2 instead of R_3. Step III describes a transition state where the geometry is that of step II while the wavefunction is that of the final Step IV. The increase in the HOMO energy by changing the wavefunction at the geometry corresponding to ~1.8 GPa is only 0.06 eV. By contrast, the energy decrease due to the ligand relaxation process on passing from step III to the final step is of 0.21 eV.

© 2022 The Authors. Chemistry - A European Journal published by Wiley-VCH GmbH

15213765, 2022, 43, Downloaded from https://chemistry-europe.onlinelibrary.wiley.com/doi/10.1002/chem.202200948 by Universidad De Cantabria, Wiley Online Library on [21/03/2024]. See the Terms and Conditions (https://onlinelibrary.wiley.com/terms-and-conditions) on Wiley Online Library for rules of use; OA articles are governed by the applicable Creative Commons License

At the same time, on passing from step I to step II the energy of the HOMO level experiences an increase of 0.63 eV (Figure 3).

The calculated HOMO wavefunction for step IV (Figure 3)

$$|\psi_H(\mathrm{IV})\rangle = 0.738|3z^2\text{-}r^2\rangle + 0.674\,|x^2\text{-}y^2\rangle \tag{4}$$

involves changes with respect to that of step II which are better seen writing $|\psi_H(\mathrm{IV})\rangle$ in the $\{|3y^2\text{-}r^2\rangle, |x^2\text{-}z^2\rangle\}$ basis

$$|\psi_H(\mathrm{IV})\rangle = 0.948\,|3y^2\text{-}r^2\rangle + 0.302|x^2\text{-}z^2\rangle \tag{5}$$

Accordingly, in $|\psi_H(\mathrm{IV})\rangle$ there is a 90% contribution of $|3y^2\text{-}r^2\rangle$ and thus the associated density lies mainly along the R_2 direction.

To calculate the energy of the HOMO level in the virtual step III we have expressed the orbital wavefunction $|\psi_H(\mathrm{IV})\rangle$ (Eq. (4)) in terms of that of the HOMO at step II, $|\psi_H(\mathrm{II})\rangle$, and its LUMO, $|\psi_L(\mathrm{II})\rangle$. As $<\psi_L(\mathrm{II})\;|\psi_H(\mathrm{II})\rangle = 0$ and the HOMO-LUMO separation in step II is equal to 0.54 eV, this means that, on passing from step II to step III (Figure 3) which represents just a change in basis, the increase in HOMO energy can be estimated to be only 0.06 eV. This slight increase reflects the relative closeness of $|\psi_H(\mathrm{IV})\rangle$ and $|\psi_H(\mathrm{II})\rangle$ as $<\psi_H(\mathrm{II})|\psi_H(\mathrm{IV})\rangle$ is equal to 0.944 from Eqs. (3) and (4). Interestingly, the 0.06 eV energy increase obtained on passing from step II to step III is widely compensated by the decrease of 0.21 eV due to the subsequent ligand relaxation involved in the transition from step III to step IV such as it is shown on Figure 3.

If the long axis switch in Na_3MnF_6 is strongly influenced by the electronic ground state of the involved MnF_6^{3-} unit a different situation would happen in Na_3FeF_6, where a more spherical electronic density around Fe^{3+} is expected to take place. Calculations carried out for Na_3FeF_6 at a pressure of 2.79 GPa support this idea. Indeed, the obtained pattern of metal-ligand distances (R_1 = 1.922 Å, R_2 = 1.935 Å and R_3 = 1.932 Å) is similar to that derived at zero pressure (Table 4) although all of them are reduced by ~0.01 Å.

It is worth noting that the switch phenomenon analyzed in Na_3MnF_6 is different from that observed[2,54] in Tutton salts like $(ND_4)_2Cu(D_2O)_6(SO_4)_2$ or $(NH_4)_2Cu(H_2O)_6(SO_4)_2$. As it has recently been shown,[17,55] the structure of $Cu(D_2O)_6^{2+}$ or $Cu(H_2O)_6^{2+}$ units in those salts at ambient pressure arises from a *compressed* geometry, with Z as principal axis and an unpaired electron in a $|3z^2\text{-}r^2\rangle$ orbital, followed by an orthorhombic *instability* in the XY plane. Accordingly, the three metal-ligand distances are ordered as follows: $R_Y > R_X > R_Z$ where R_Y and R_X stand for the Cu–O_8 and Cu–O_7 bonds respectively while R_Z corresponds to the shortest Cu–O_9 bond. Interestingly, despite the orthorhombic distortion, the wavefunction of the unpaired electron at ambient pressure keeps an 82% of $3z^2$-r^2 character.[17] Upon raising the applied pressure at 0.15 GPa the long axis is no longer the Cu–O_8 but the Cu-O_7 bond[2,54] thus implying $R_X > R_Y > R_Z$ with R_Z being unmodified within 1%. For this reason, in the switch process corresponding to $(ND_4)_2Cu(D_2O)_6(SO_4)_2$ or $(NH_4)_2Cu(H_2O)_6(SO_4)_2$ the unpaired electron wavefunction *maintains* a dominant $3z^2$-r^2 character[17] a situation distinct to that encountered in Na_3MnF_6.

Optical transitions of Na_3MnF_6 at ambient and high pressure

The ground state, Ψ_0, with S = 2 and M_S = 2, of a high spin d^4 complex can shortly be written by the following Slater determinant

$$\Psi_0 = |\, xz\uparrow yz\uparrow xy\uparrow 3z^2\text{-}r^2\uparrow\; | \tag{6}$$

Accordingly, the spin allowed excitations involve jumps from the four orbitals appearing in Ψ_0 to the empty $|x^2\text{-}y^2\rangle$ orbital and thus they are the most intense among the *d-d* transitions coming from Cr^{2+} or Mn^{3+} complexes.[56,57,28]

In the case of Na_3MnF_6 at ambient pressure the values of such spin allowed transitions have been reported by Palacio and Moron[57] and Carlson et al.[1] although the last authors have not detected the lowest transition $3z^2\text{-}r^2\uparrow \rightarrow x^2\text{-}y^2\uparrow$. Experimental transition energies are collected in Table 6 and compared to the values obtained in the present calculations. The calculated *d-d* transitions are reasonably close to those observed experimentally at ambient pressure.

It is worth noting now that in K_3MnF_6 there are two different Mn^{3+} sites[58] and the geometry of the so-called Mn^{3+}(2) site is very close to that found in Na_3MnF_6 at ambient pressure (Table 1). Indeed, the values of R_1, R_2, and R_3 differ by less than 3%, and the value of the average metal-ligand distance, $\langle R\rangle$, is equal in both cases to 1.93 Å.[1,58] The experimental d-d excitations measured in a powder K_3MnF_6 for the Mn^{3+}(2) site[58] are close to those reported for Na_3MnF_6 in Table 6, the differences being smaller than 12%.

For the sake of completeness, we have compared the *d-d* transitions for Na_3MnF_6[1,57] and CrF_2[56] (involving $3d^4$ cations, Mn^{3+} and Cr^{2+}) measured at ambient pressure. The three transitions coming from {xy, xz, yz} levels are clearly higher for Na_3MnF_6[1,57] than for CrF_2.[56] For instance, the highest *d-d* transition for Na_3MnF_6 is found at ~2.45 eV and only at 1.75 eV for CrF_2 as shown in Table 7. This fact partially reflects the higher value of $\langle R\rangle$ for CrF_2 than for Na_3MnF_6. For this reason, it may be surprising that the opposite happens for the lowest *d-d* transition (Table 7) as it is equal to 1.04 eV for Na_3MnF_6[57] while equal to 1.22 eV for CrF_2.[56,28] Nevertheless, the CrF_6^{4-} unit in CrF_2 is, in principle, compressed along the z direction but followed by an orthorhombic instability[28] leading to a significant difference of final Cr^{2+}–F^- distances along *x* (R_1) and *y* (R_2)

Table 6. Calculated optical transitions for Na_3MnF_6 at ambient pressure. They are compared to the experimental values reported by Palacio and Moron (I) and Carlson et al. (II). Energies are all given in eV units.

Optical Transition	Calculated	Experim. (I)	Experim. (II)
$\|3z^2\text{-}r^2\rangle \rightarrow \|x^2\text{-}y^2\rangle$	0.71	1.04	–
$\|xy\rangle \rightarrow \|x^2\text{-}y^2\rangle$	2.11	2.18	2.17
$\|yz\rangle \rightarrow \|x^2\text{-}y^2\rangle$	2.27	2.38	2.38
$\|xz\rangle \rightarrow \|x^2\text{-}y^2\rangle$	2.32	2.38	2.58

© 2022 The Authors. Chemistry - A European Journal published by Wiley-VCH GmbH

15213765, 2022, 43, Downloaded from https://chemistry-europe.onlinelibrary.wiley.com/doi/10.1002/chem.202200948 by Universidad De Cantabria, Wiley Online Library on [21/03/2024]. See the Terms and Conditions (https://onlinelibrary.wiley.com/terms-and-conditions) on Wiley Online Library for rules of use; OA articles are governed by the applicable Creative Commons License

Table 7. Experimental values (in eV) of highest, E_H, and lowest, E_L, *d-d* transitions for CrF_2[56] and Na_3MnF_6[57,1] measured at ambient pressure. The values of the average metal-ligand distance, $\langle R \rangle$, and $|R_2\text{-}R_1|$ (in Å units) are also given.

	E_H	E_L	$< R >$	$\lvert R_2\text{-}R_1 \rvert$
CrF_2	1.75	1.22	2.14	0.42
Na_3MnF_6	~2.45	1.01	1.94	0.01

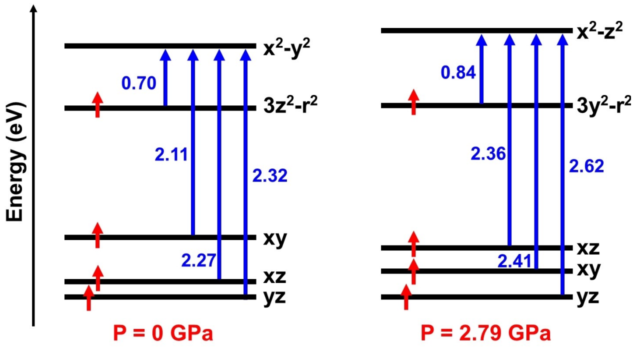

Figure 4. Energies (in eV) of spin allowed *d-d* transitions of Na_3MnF_6 calculated for a MnF_6^{3-} complex with the experimental geometries at $P = 0$ and $P = 2.79$ GPa. The dominant contribution for each orbital is shown, and the spin distribution corresponds to the electronic ground state ($S = 2$, $M_S = 2$). Note that on passing from ambient pressure to $P = 2.79$ GPa, the nature of HOMO and LUMO orbitals has been modified as well as the order of three levels coming from t_{2g} in O_h symmetry.

directions equal to 0.416 Å (Table 7). As shown in Ref. [28] the existence of this huge orthorhombic distortion increases the value of the $x^2\text{-}y^2\uparrow \rightarrow 3z^2\text{-}r^2\uparrow$ transition in CrF_2 by 0.60 eV.

Concerning the influence of pressure upon *d-d* excitations we have also calculated the values of four spin allowed transitions of Na_3MnF_6 at $P = 2.79$ GPa. Results are depicted in Figure 4 and compared to those obtained for zero pressure. In accord with results of section 4.3, the nature of HOMO and LUMO orbitals has been modified as well as the order of three levels coming from t_{2g} in O_h symmetry (Figure 4). The present results shed light on the three optical transitions measured by Carlson et al. in the high-pressure phase of Na_3MnF_6.[1] Indeed, according to Figure 4, the peaks observed at 2.19 eV, 2.39 eV and 2.59 eV by Carlson et al. can reasonably be assigned to the $xz\uparrow \rightarrow x^2\text{-}z^2\uparrow$, $xy\uparrow \rightarrow x^2\text{-}z^2\uparrow$ and $yz\uparrow \rightarrow x^2\text{-}z^2\uparrow$ excitations, respectively. As shown in Figure 4, the HOMO-LUMO gap is calculated to increase by 0.14 eV on going from $P = 0$ to $P = 2.79$ GPa, a fact that is partially helped by the increase of orthorhombicity. Indeed, while at $P = 2.79$ GPa $R_3\text{-}R_1 = 0.168$ Å, at ambient pressure $R_1\text{-}R_2$ is equal only to 0.035 Å (Table 1). Unfortunately, in the experimental set-up by Carlson et al. the absorption measurements under pressure were carried out for photon energies above 1.5 eV[1] and thus the lowest *d-d* transition has not been detected.

Conclusions

The present results show the usefulness of the parent phase as a good starting point for understanding the behavior of low symmetry compounds containing d^n ($n = 4$, 9) cations. In the present case, when we introduce a substitutional Mn^{3+} impurity in the parent Na_3FeF_6 compound, the HOMO wavefunction is already determined by the low local symmetry, which in turn, fixes the subsequent distortion due to an electron density that exerts a different force on the three kinds of ligands. Moreover, the force constant for moving a ligand is different in each type of ligands as a result of the low symmetry of the lattice. This behavior has been well studied in layered lattices like K_2MF_4 ($M = Mg$, Zn) doped with d^9 ions like Cu^{2+} or Ni^+.[26,32]

Bearing these facts in mind, we can now envisage the differences and similarities between low symmetry and JT systems. If we place a d^4 cation in a cubic material with sixfold coordination, the ground state is degenerate, and thus the e_g electron is, in general, described by a linear combination of $|3z^2\text{-}r^2\rangle$ and $|x^2\text{-}y^2\rangle$ molecular orbitals of the associated complex. If the unpaired electron is located in the $|3z^2\text{-}r^2\rangle$ orbital the corresponding adiabatic minimum corresponds to a tetragonal elongated complex while it is compressed if placed in $|x^2\text{-}y^2\rangle$. Usually for systems displaying a static JT effect the elongated conformation is preferred,[9,19] with the known exception of $CaO:Ni^+$ which is compressed,[59] a matter discussed in Ref. [60]. Nevertheless, if the complex is tetragonal elongated, there are still three different possibilities for the electronic ground state of the complex because of the cubic symmetry. Indeed, the electron wavefunction can be either $|3z^2\text{-}r^2\rangle$, $|3x^2\text{-}r^2\rangle$ or $|3y^2\text{-}r^2\rangle$. In real crystals, this equivalence is, however, often destroyed by small random strains, establishing one of the three initially degenerate options *at a given point* of the lattice.[9] Once the unpaired electron is then *fixed* in the $|3z^2\text{-}r^2\rangle$ orbital, the corresponding electron density does not exhibit cubic symmetry and thus, induces a tetragonal distortion.[53] This behavior is usually called a static JT effect[9,10] well observed in cases like $KZnF_3:Cu^{2+}$[11,12] or d^9 ions (Ni^+, Cu^{2+}, Ag^{2+}) in alkali halides.[14–20,33] Nevertheless, when random strains play a minor role, there is no symmetry breaking, and EPR spectra of JT systems exhibit a cubic and not a tetragonal symmetry.[9,10] This uncommon phenomenon has been observed for Cu^{2+} or Ag^{2+}-doped MgO where EPR spectra[61–63] and first principle calculations[64] prove the existence of *coherent* tunneling[9,10] among equivalent adiabatic minima thus leading to a global cubic symmetry.

According to this reasoning, if we deal with a static JT effect with *z* as main axis, an applied hydrostatic pressure, which is an isotropic stress,[65] cannot destroy the equivalence between *x* and *y* axes of a tetragonal complex and thus the nature of the principal axis is unmodified. By contrast, a different situation occurs when the d^n ($n = 4$, 9) cation is placed in a low symmetry lattice where the corresponding complex shows at most an orthorhombic geometry such as it is found for Na_3MnF_6 and K_3MnF_6. Accordingly, in this circumstance, as the geometry does not arise from a JT effect, one can expect, after careful consideration of the elastic properties of the solid, possible

© 2022 The Authors. Chemistry - A European Journal published by Wiley-VCH GmbH

15213765, 2022, 43, Downloaded from https://chemistry-europe.onlinelibrary.wiley.com/doi/10.1002/chem.202200948 by Universidad De Cantabria, Wiley Online Library on [21/03/2024]. See the Terms and Conditions (https://onlinelibrary.wiley.com/terms-and-conditions) on Wiley Online Library for rules of use; OA articles are governed by the applicable Creative Commons License

15213765, 2022, 43, Downloaded from https://chemistry-europe.onlinelibrary.wiley.com/doi/10.1002/chem.202200948 by Universidad De Cantabria, Wiley Online Library on [21/03/2024]. See the Terms and Conditions (https://onlinelibrary.wiley.com/terms-and-conditions) on Wiley Online Library for rules of use; OA articles are governed by the applicable Creative Commons License

pressure-induced switches of the longest axis, such as those observed for Na_3MnF_6.[1]

In accord to present results, the properties of d^4 and d^9 low symmetry compounds with sixfold coordination cannot be explained *transferring* the E⊗e JT framework, valid for a parent cubic symmetry, to an initial tetragonal or orthorhombic symmetry.[13] For an initial cubic symmetry, the adiabatic minima have tetragonal symmetry well observed experimentally in cases displaying a static JT effect.[9–20,49,50] Thus, when the observed local symmetry of the involved complex is orthorhombic or lower, such as it happens for Na_3MnF_6, explanations based on the JT effect[2–8] are likely to be meaningless. Along this line, the existence of a switch of the JT axis recently put forward[66] for explaining the behavior of $[(CH_3)_2NH_2]Cu(HCOO)_3$ under pressure is certainly doubtful due to the monoclinic symmetry of the lattice at ambient pressure. A similar situation holds for recent results[67] on the rhombohedral CuPyr-I compound where the six ligands around Cu^{2+} are not identical (two N and four O) a fact that is already against the existence of a JT effect.

The present work stresses the importance of considering the anisotropic elastic response to pressure in low symmetry systems containing d^4 or d^9 ions. It opens a window for properly understanding the pressure effects upon insulating compounds such as $CuF_2(H_2O)_2(pyz)$[4] (pyz = pyrazine). Further work along this line is now in progress.

Acknowledgements

The authors acknowledge financial support from Grant PGC2018-096955-B–C41 funded by MCIN/AEI/10.13039/501100011033 and by "ERDF A way of making Europe", by the European Union. The support by the European Union and the University of Cantabria under FEDER project EQC2019-006136-P is also acknowledged.

Conflict of Interest

The authors declare no conflict of interest.

Data Availability Statement

The data that support the findings of this study are available from the corresponding author upon reasonable request.

Keywords: anisotropy · Jahn-Teller effect · low symmetry lattice · parent phase · pressure-induced switch

[1] S. Carlson, Y. Xu, U. Halenius, R. Norrestam, *Inorg. Chem.* **1998**, *37*, 1486–1492.
[2] C. J. Simmons, M. A. Hitchman, H. Stratemeier, A. Schultz, *J. Am. Chem. Soc.* **1993**, *115*, 11304–11311.
[3] M. Augustyniak-Jabłokow, A. Krupska, *Chem. Phys. Lett.* **2003**, *377*, 137–142.
[4] G. J. Halder, K. W. Chapman, J. A. Schlueter, J. L. Manson, *Angew. Chem. Int. Ed.* **2011**, 50, 419–421; *Angew. Chem.* **2011**, *123*, 439–441.
[5] J. Ruiz-Fuertes, A. Segura, F. Rodríguez, D. Errandonea, M. N. Sanz-Ortiz, *Phys. Rev. Lett.* **2012**, *108*, 166402.
[6] U. Englich, W. Massa, A. Tressaud, *Acta Crystallogr. Sect. C* **1992**, *48*, 6–8.
[7] N. Charles, J. M. Rondinelli, *Phys. Rev. B* **2014**, 90, 094114(R).
[8] M. A. Halcrow, *Chem. Soc. Rev.* **2013**, *42*, 1784–1795.
[9] F. S. Ham, *Electron Paramagnetic Resonance* (Ed.: S. Geschwind), Plenum, New York, **1972**.
[10] P. García-Fernández, A. Trueba, M. T. Barriuso, J. A. Aramburu, M. Moreno, *Prog. Theor. Chem. Phys.* **2011**, *23*, 105–142.
[11] E. M. C. Minner, Etude Spectroscopique des Ions Jahn–Teller Cuivre et Argent Bivalents dans des Monocristaux de Fluoroperovskites de Composition Chimique AMF_3, PhD thesis, University of Geneva, **1993**.
[12] L. Dubicki, M. J. Riley, E. R. Krausz, *J. Chem. Phys.* **1994**, *101*, 1930–1938.
[13] J. A. Aramburu, P. García-Fernández, J. M. García-Lastra, M. Moreno, *J. Phys. Chem. C* **2017**, *121*, 5215–5224.
[14] A. Shengelaya, H. Drulis, B. Macalik, M. Suzynska, *Z. Phys. B* **1997**, *101*, 373–376.
[15] M. T. Barriuso, B. Ortiz-Sevilla, J. A. Aramburu, P. Garcia-Fernandez, J. M. García-Lastra, M. Moreno, *Inorg. Chem.* **2013**, *52*, 9338–9348.
[16] R. H. Borcherts, H. Kanzaki, H. Abe, *Phys. Rev. B: Solid State* **1970**, *2*, 23–27.
[17] J. A. Aramburu, A. Bhowmik, J. M. García-Lastra, P. García-Fernández, M. Moreno, *J. Phys. Chem. C* **2019**, *123*, 3088–3101.
[18] J. Sierro, *J. Phys. Chem. Solids* **1967**, *28*, 417–422.
[19] H. Bill, *The Dynamical Jahn-Teller Effect in Localized Systems* (Eds.: Y. E. Perlin, M. Wagner), Elsevier, Amsterdam, **1984**.
[20] A. Trueba, J. M. García-Lastra, C. de Graaf, P. García-Fernández, J. A. Aramburu, M. T. Barriuso, M. Moreno, *Chem. Phys. Lett.* **2006**, *430*, 51–55.
[21] B. Bleaney, K. D. Bowers, R. S. Trenam, *Proc. R. Soc. London Ser. A* **1955**, 228, 157–166.
[22] L. S. Dang, R. Buisson, F. I. B. Williams, *J. Physique (Paris)* **1974**, *35*, 49–65.
[23] R. S. Rubins, L. N. Tello, D. K. De, T. D. Black, *J. Chem. Phys.* **1984**, *81*, 4230–4233.
[24] I. Sánchez-Movellán, J. Moreno-Ceballos, P. García-Fernández, J. A. Aramburu, M. Moreno, *Chem. Eur. J.* **2021**, *27*, 13582–13590.
[25] Z. Mazej, D. Kurzydłowski, W. Grochala, *Photonic and Electronic Properties of Fluoride Materials* (Eds.: A. Tressaud, K. Poeppelmeier), Elsevier, Amsterdam, **2016**, p. 231–260.
[26] J. A. Aramburu, J. M. García-Lastra, P. García-Fernández, M. T. Barriuso, M. Moreno, *Inorg. Chem.* **2013**, *52*, 6923–6933.
[27] D. Babel, A. Tressaud, *Inorganic Solid Fluorides* (Ed: P. Hagenmuller), Academic Press, New York, **1985**.
[28] J. A. Aramburu, M. Moreno, *Phys. Chem. Chem. Phys.* **2019**, *21*, 11714–11723.
[29] J. A. Aramburu, P. García-Fernández, N. R. Mathiesen, J. M. García-Lastra, M. Moreno, *J. Phys. Chem. C* **2018**, *122*, 5071–5082.
[30] M. J. Riley, L. Dubicki, G. Moran, E. R. Krausz, *Chem. Phys.* **1990**, *14*, 363–373.
[31] R. Alcala, E. Zorita, P. J. Alonso, *J. Phys. C* **1988**, *21*, 461–470.
[32] J. M. García-Lastra, J. A. Aramburu, M. T. Barriuso, M. Moreno, *Phys. Rev. Lett.* **2004**, *93*, 226402.
[33] I. Sánchez-Movellán, J. A. Aramburu, M. Moreno, *Phys. Chem. Chem. Phys.* **2020**, *22*, 7875–7887.
[34] F. C. Hawthorne, R. B. Ferguson, *Can. Mineral.* **1975**, *13*, 377–382.
[35] R. Dovesi, et al. CRYSTAL17 User's Manual (University of Torino, Torino), **2017**.
[36] M. F. Peintinger, D. V. Oliveira, T. J. Bredow, *J. Comput. Chem.* **2013**, *34*, 451–459.
[37] CRYSTAL basis sets. https://www.crystal.unito.it/basis-sets.php (accessed on May 29, 2021) .
[38] T. Bredow, A. Gerson, *Phys. Rev. B* **2000**, *61*, 5194–5201.
[39] R. D. Shannon, *Acta Crystallogr.* **1976**, *A32*, 751–767.
[40] G. te Velde, F. M. Bickelhaupt, E. J. Baerends, C. F. Guerra, S. J. van Gisbergen, J. D. Snijders, T. Ziegler, *J. Comput. Chem.* **2001**, *22*, 931–967.
[41] M. Moreno, J. A. Aramburu, M. T. Barriuso, *Struct. Bonding* **2004**, *106*, 127–152.
[42] M. J. Colaneri, J. Vitali, *J. Phys. Chem. A* **2021**, *125*, 3268–3278.
[43] W. Van Gool, A. G. Piken, *J. Mater. Sci.* **1969**, *4*, 95–104.
[44] M. P. Tosi, *Solid State Phys.* **1964**, *16*, 1–120.
[45] J. M. García-Lastra, M. T. Barriuso, J. A. Aramburu, M. Moreno, *Phys. Rev. B* **2009**, *79*, 241106(R).

© 2022 The Authors. Chemistry - A European Journal published by Wiley-VCH GmbH

[46] M. O. J. Hunault, Y. Harada, J. Miyawaki, J. Wang, A. Meijerink, F. M. F. de Groot, *J. Phys. Chem. A* **2018**, *122*, 4399–4413.
[47] J. A. Aramburu, P. García-Fernández, J. M. García-Lastra, M. T. Barriuso, M. Moreno, *J. Phys. Condens. Matter* **2013**, *25*, 175501–17558.
[48] P. García-Fernández, M. Moreno, J. A. Aramburu, *Inorg. Chem.* **2015**, *54*, 192–199.
[49] H. Vercammen, D. Schoemaker, B. Briat, F. Ramaz, F. Callens, *Phys. Rev. B* **1999**, *59*, 11286–11292.
[50] M. T. Barriuso, P. García-Fernández, J. A. Aramburu, M. Moreno, *Solid State Commun.* **2001**, *120*, 1–5.
[51] J. A. Aramburu, M. Moreno, *Inorg. Chem.* **2019**, *58*, 4609–4618.
[52] W. J. Croft, M. Kestigian, *Mat. Res. Bull.* **1968**, *3*, 571–575.
[53] J. M. García-Lastra, M. T. Barriuso, J. A. Aramburu, M. Moreno, *Chem. Phys.* **2005**, *317*, 103–110.
[54] A. J. Schultz, M. A. Hitchman, J. D. Jorgensen, S. Lukin, P. A. Radaelli, C. J. Simmons, H. Stratemeier, *Inorg. Chem.* **1997**, *36*, 3382–3385.
[55] D. C. Peets, M. Avdeev, M. C. Rahn, F. Pabst, S. Granovsky, M. Stötzerand, D. S. Inosov, *ACS Omega* **2022**, 7, 5139–5145.
[56] P. E. Lim, J. W. Stout, *J. Chem. Phys.* **1975**, *63*, 4886–4902.
[57] F. Palacio, M. C. Morón, *Magneto-Structural Correlations in Mn(III) Fluorides, in Research Frontiers in Magneto Chemistry* (Ed.: C. J. O'Connor), World Scientific, **1993**.
[58] C. Stoll, M. Atanasov, J. Bandemehr, F. Neese, C. Pietzonka, F. Kraus, A. J. Karttunen, M. Seibald, G. Heymann, H. Huppertz, *Chem. Eur. J.* **2021**, *27*, 9801–9813.
[59] W. Low, J. T. Suss, *Phys. Lett.* **1963**, *7*, 310–312.
[60] J. A. Aramburu, P. García-Fernández, J. M. García-Lastra, M. Moreno, *ChemPhysChem* **2016**, *17*, 2146–2156.
[61] R. E. Coffman, *J. Chem. Phys.* **1968**, *48*, 609–618.
[62] L. A. Boatner, R. W. Reynolds, Y. Chen, M. M. Abraham, *Phys. Rev. Lett.* **1973**, *31*, 7–10.
[63] M. J. Riley, C. J. Noble, P. L. W. Tregenna-Piggott, *J. Chem. Phys.* **2009**, *130*, 104708.
[64] P. García-Fernández, A. Trueba, M. T. Barriuso, J. A. Aramburu, M. Moreno, *Phys. Rev. Lett.* **2010**, *104*, 035901.
[65] L. D. Landau, E. M. Lifshitz, *Theory of Elasticity*, 2nd edition, Pergamon Press, **1970**, p. 12.
[66] R. Scatena, M. Andrzejewski, R. D. Johnson, P. Macchi, *J. Mater. Chem. C* **2021**, *9*, 8051–8056.
[67] Ch. J. McMonagle, P. Comar, G. S. Nichol, D. R. Allan, J. Gonzalez, J. A. Barreda-Argüeso, F. Rodríguez, R. Valiente, G. F. Turner, E. K. Brechin, S. A. Moggach, *Chem. Sci.* **2020**, *11*, 8793–8799.

Manuscript received: March 28, 2022
Accepted manuscript online: May 30, 2022
Version of record online: June 14, 2022

© 2022 The Authors. Chemistry - A European Journal published by Wiley-VCH GmbH

15213765, 2022, 43, Downloaded from https://chemistry-europe.onlinelibrary.wiley.com/doi/10.1002/chem.202200948 by Universidad De Cantabria, Wiley Online Library on [21/03/2024]. See the Terms and Conditions (https://onlinelibrary.wiley.com/terms-and-conditions) on Wiley Online Library for rules of use; OA articles are governed by the applicable Creative Commons License